Regional analysis of neutron/gamma event anisotropy using a multi-anode photomultiplier tube

P M Collins-Price1*, M J Joyce1

¹ School of Engineering, Lancaster University, Lancaster, UK

*E-mail: p.collins-price@lancaster.ac.uk

Abstract. This study demonstrates real-time centre-of-interaction coordinate measurements which can be performed alongside simultaneous pulse analysis, showing anisotropy in full-volume event data. This event anisotropy is shown to be dependent on incident radiation type, with neutron counts favouring the centre of the coordinate readout. This allows for flexible event selection based on regional pulse behaviour, eliminating the need for arbitrary and indiscriminate energy thresholds for PSD. On this basis it is anticipated that FoM might instead be optimised in-field according to situational needs, allowing more accurate measurements across the full spectrum capabilities of the detector and therefore improving the efficacy of established nuclear detection and monitoring methods.

1. Introduction

1.1 Mixed-field neutron detection

Detecting neutrons accurately is vital for nuclear safeguards and security, special nuclear material (SNM) assay, and reactor monitoring. Organic scintillation detectors sensitive to both gamma and neutron events are used widely for their resilience and rapid timing characteristics.

Pulse-shape discrimination (PSD) allows events to be separated into gamma and neutron plumes [1]. However, these plumes can be broad, and challenges can arise at lower energies \Rightarrow 500 keV where the neutron and gamma plumes tend to overlap [1][2][3]. The degree of separation between the plumes is characterised by a figure-of-merit (FoM) expressed as the separation of the neutron and gamma event plumes divided by the sum of their respective widths.

This parameter can be artificially improved via energy cut-offs, which exclude the low-energy overlap zone somewhat arbitrarily, in a manner that inherently reduces the overall detection efficiency and invalidates the FoM for low-energy fields. The field with which the FoM is derived also affects this, since high-energy fields such as from americium-beryllium can yield better separation than, say, californium-252 for which the overlapping event intensity is greater^{[3][4]}. The stated FoM may therefore not be representative of neutron fluxes encountered typically in nuclear safeguarding or SNM monitoring environments.

1.2 Scintillator geometry

Scintillator geometry significantly affects light-collection efficiency^[5] (LCE), which in turn determines critical performance metrics such as particle-type identification ^{[6][7]}, particularly so for low-energy events that emit less light where PSD FoM is significantly worsened^[1]. Energy resolution is also impacted^[8], as maximizing the collection of emitted light is essential to increasing the sensitivity of the detector to small differences in light output between events.

Content from this work may be used under the terms of the Creative Commons Attribution 4.0 licence. Any further distribution of this work must maintain attribution to the author(s) and the title of the work, journal citation and DOI.

Past research has studied how scintillator geometry effects FoM^{[5][6][7][8]} and spatial variations in scintillation pulse height^[9], but the impact of centre-of-interaction location on events within the scintillator itself, particularly regarding PSD performance, has not been investigated. Optimising FoM by selectively analysing events within favourable scintillator regions may enable improved discrimination accuracy and efficiency in a more objective manner.

1.3 MAPMT readout

MAPMTs have traditionally been employed for Anger cameras [10][11], directional gamma sensors [12][13], or alongside pixelated scintillators [14][15] or optical fibres [16] for high-resolution particle detection. These commonly use charge division [10][14] to locate interactions. Prior studies have focused on imaging [10][11] and spatial measurements such as time-of-flight [12][17] rather than using the MAPMT to assess regional properties of light behaviour within the scintillator itself.

2. Methods

2.1 Detector setup

The detector comprised a 49x49x10 mm EJ-276 scintillator cell coupled to a Hamamatsu H13700 multi-anode photomultiplier tube (MAPMT) with a Vertilon SIB71256 resistor matrix readout. The four Anger logic outputs were measured on a 4-channel Agilent Infiniium MSO8104A oscilloscope connected to the host PC by ethernet, with real-time data acquisition and processing performed in MATLAB through a VISA instrument object. Each pulse was background corrected and smoothed using a rolling average to suppress signal noise.

2.2 Coordinate readout

The position resolution of the detector was verified by placing a vertical slit collimator, a horizontal slit collimator, and a circular aperture between the ¹³⁷Cs source and the detector face, each formed from 50 mm thick lead blocks. The resulting coordinate heatmaps of measured interaction location are shown in Figure 1. The expected interaction regions, shown in white, were calculated from the collimator geometry to qualitatively illustrate coordinate fidelity.

Pixel dimensions are determined dynamically by binning the x and y coordinates of the total measured dataset into histograms following the Freedman-Diaconis rule^[18]. This ensures a consistent balance between resolution and counting statistics, both improving for higher counts.

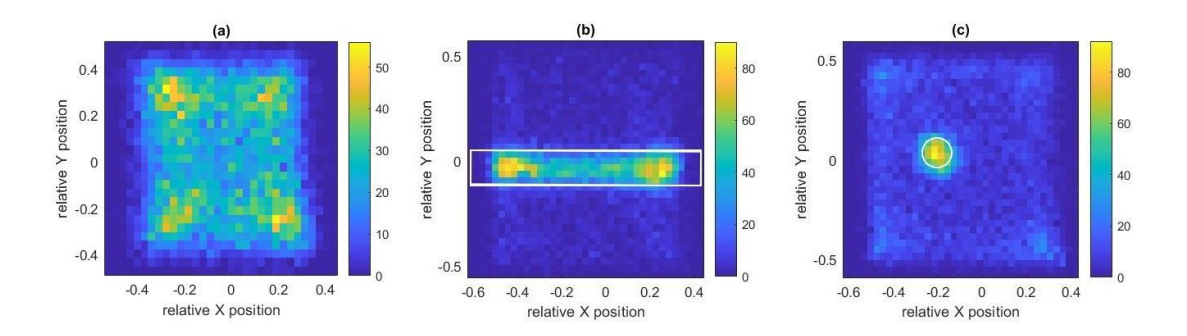


Figure 1. Coordinate heatmaps for (a) no collimator, (b) a 3 mm horizontal slit collimator with 85 mm source/detector separation, and (c) a 4 mm circular aperture with 70 mm source/detector separation. Power cable placement made the vertical measurement slightly askew. The colour scale shows event counts per pixel for each plot.

Anisotropy is seen in Figure 1 (a) and (b) with more events recorded at the peripheries of the distributions and almost no events being recorded at coordinates outside the ranges -0.58 < Xpos < 0.44 and -0.58 < Ypos < 0.58. If light collection were unaffected by the scintillator geometry, or confined close to the centre of interaction (CoI) e.g. in a pixellated scintillator^{[14][15]}, the Anger-logic equation would return a theoretically uniform distribution of coordinates ranging from -1 to +1 in x and y[10], however this is not observed with the continuous scintillator used here which suggests that events with true interaction coordinates close to the scintillator walls are "piling up" at measured coordinate values closer to the origin.

2.3 Internal reflection Monte-Carlo simulation

To test this proposed explanation, a Monte-Carlo simulation was performed modelling events occurring within the full coordinate space and comparing the measured CoI responses between a theoretical infinitely large detector with no internal reflection and a clearly more physical finite scintillator with internally reflective top and side faces. The modelled finite scintillation cell dimensions were the same as the scintillator used for the real measurements.

The simulation first randomly generated 100,000 uniformly distributed "true" interaction locations with x and y values between -1 and +1. For each event, 500 random light samples were taken with radial length r and angle θ . In the case of a boundless detector, the x and y coordinates where each light sample was collected on the MAPMT face are $x_{scintillation} = x_{event} + r \cdot Cos\theta$ and $y_{scintillation} = y_{event} + r \cdot Sin\theta$. For the bounded, internally reflective scintillator cell the calculations were the same except the resulting values for $x_{scintillation}$ and $y_{scintillation}$ were then passed through a function that reflected them at the scintillator boundaries if they had absolute value > 1. For example, the sampling coordinate value +0.7 would be unchanged, whereas the sampling coordinate value -1.2 would become -0.8 after reflection.

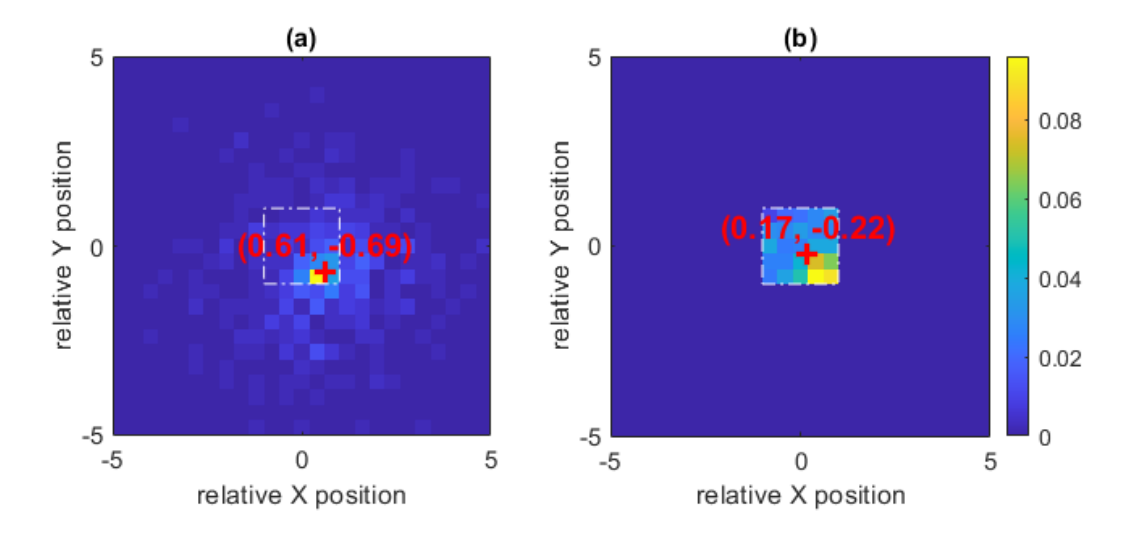


Figure 2. Simulated light dispersion and measured CoI in red for (a) an infinite detector with no scintillator boundaries and (b) a finite detector with an internally reflective scintillator. The outline of the full Anger logic coordinate space is shown as a white dotted line. In (b) this marks the reflective boundary that "folds" the scintillation pulse back over itself, causing its CoI to be measured closer to the origin from its true position. The boundary in (a) has no effect but is shown to aid comparison. The colour scale shows probability-normalised light collection intensity.

In both cases, the CoI coordinates of each event were calculated by taking the mean of these randomly generated x and y light samples. Figure 2 shows an example of how the measured CoI coordinate of a single event changes due to the modelled internal reflection, as the folding of the light distribution causes the measured CoI coordinate of an event close to the reflective boundary to be pushed towards the centre of the scintillator. The resulting difference between the expected and observed normalised distributions of 100,000 events with no collimation is modelled in Figure 3, demonstrating how the hotspots observed in the real detector data in Figure 1 arise, while Figure 4 shows the same simulated for the slit and hole collimators.

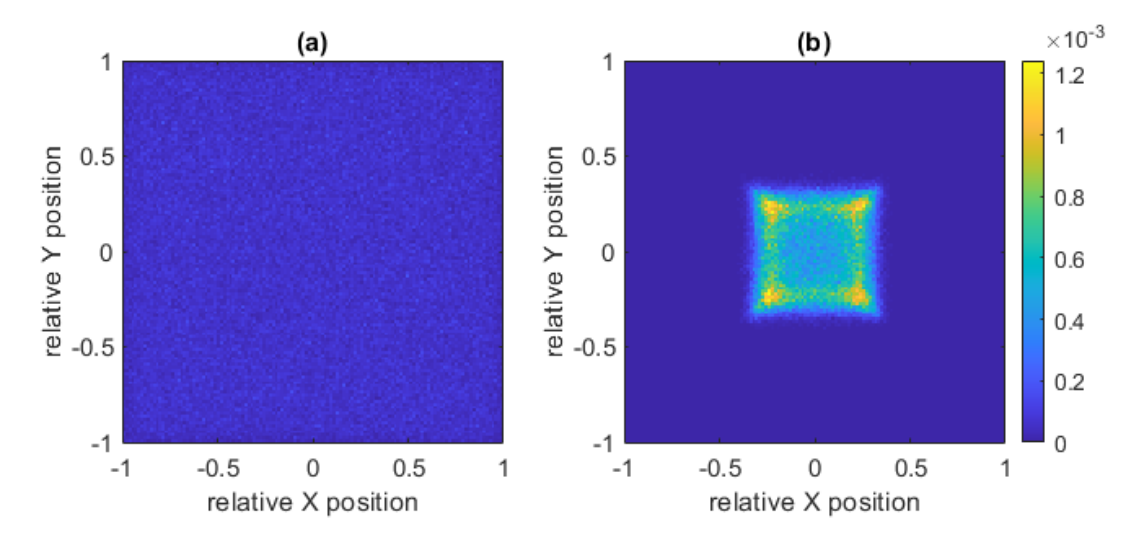


Figure 3. Heatmaps showing the modelled CoI distributions from the Monte-Carlo simulations of 100,000 uniformly distributed events with no collimation for (a) an infinite detector with no scintillator boundaries and (b) a finite detector with an internally reflective scintillator. Both distributions are normalised by probability to the same colour scale, showing how the observed regions of higher measured count intensity arise due to internal reflection "folding" the scintillation light pulses. The colour scale shows probability-normalised event intensity per pixel.

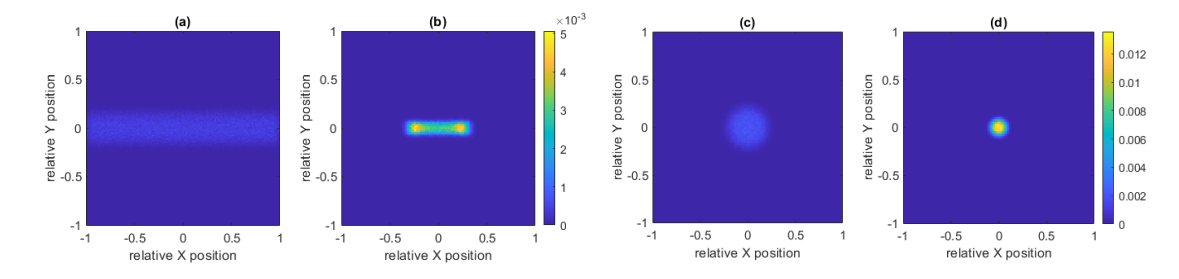


Figure 4. Heatmaps (a) and (c) show modelled event distributions for an infinite detector with no scintillator boundaries and events incident through a slit or hole collimator respectively, while (b) and (d) respectively show the modelled event distributions for a finite detector with an internally reflective scintillator and the same collimator. Again, the observed regions of higher measured count intensity can be observed at the ends of the slit region and the centre of the round aperture. Only events incident directly through the collimator were modelled, hence why there is no noise in the Monte-Carlo distributions compared to the real measured distributions for each setup.

Journal of Physics: Conference Series 3130 (2025) 012006

doi:10.1088/1742-6596/3130/1/012006

3. Results

3.1 Mixed-field anisotropy

The modelled data suggests that the observed event anisotropy is largely attributable to the behaviour of scintillation light pulses within the scintillator. This in turn raises the possibility that neutron and gamma events, each producing different scintillation profiles, may exhibit distinct anisotropy patterns due to differing internal reflection behaviours.

The event type dependency was investigated using the mixed field from a 252 Cf neutron tank. The detector was placed 50 mm from the active face of the tank in a high-density polyethylene (HDPE) case leaving the front face of the detector exposed. The voltage range was set to allow the full emission spectrum to be measured. Two sets of measurements were taken:

- 1) gamma-dominated field, with the source extended and 50 mm of HDPE shielding;
- 2) mixed field, with the source extended and 50 mm of lead shielding. Coordinate heatmaps for each of these fields are shown in Figure 5 (a) and (b) respectively.

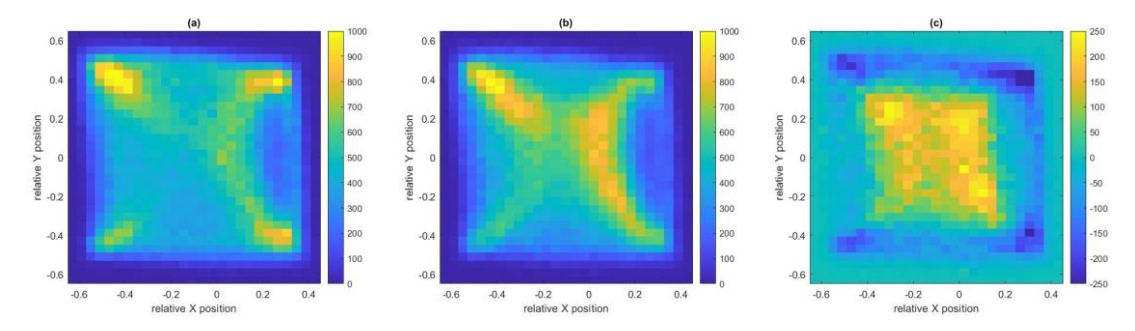


Figure 5. Coordinate heatmaps for each of the measurements made in front of the neutron tank with (a) 50 mm of HDPE shielding to reduce the neutron flux, and (b) with 50 mm lead shielding to attenuate gamma rays and increase neutron counts. Plots (a) and (b) are normalised to the same colour scale showing non-discriminated event counts per pixel, and each shows a clear and distinct anisotropy in measured CoI coordinates. Increased neutron flux results in increased count intensity in the centre of the measured distribution, with the difference (b-a) shown in (c).

3.2 Event-type dependency

To quantify this variation in anisotropy between event types, both heatmaps were produced using identical 2D histogram bins so that a Chi-squared test could be performed in MATLAB R2021a. The gamma-dominated data was used as the *expected* values and the increased neutron flux data as the *observed* values. 789 bin pairs had counts ≥ 5 for both distributions, from which a Chi-squared value of 16352.07 was calculated with 788 degrees-of-freedom. This gives a p-value of 0 or, more precisely, below the machine precision used to calculate it. The two measured event distributions can therefore be safely said to be statistically significantly distinct.

These observations show a real anisotropy in measured event data that varies depending on incident radiation type. This anisotropy can therefore be exploited to improve neutron counting power by selectively reading from sections of the scintillator that demonstrate favourable collection of neutron events over competing gamma background. The detector system described here is now being used alongside a newly acquired 8-channel oscilloscope to measure CoI coordinates alongside full pulse data to investigate possible improvements to neutron-gamma PSD, to be published later once data analysis is complete.

Journal of Physics: Conference Series 3130 (2025) 012006

doi:10.1088/1742-6596/3130/1/012006

4. Conclusion

The novel use of a 16×16 multi-anode photomultiplier tube (MAPMT) to extract centre-of-interaction coordinate information from a continuous scintillator in real time has been demonstrated. Measurements of a 252 Cf mixed field showed variation in event anisotropy between neutron and gamma fluxes, enabling subsequent work to quantify the FoM in contrasting regions of the scintillator volume.

Both neutron and gamma events exhibit anisotropy of the light response within a continuous scintillator, with neutron count intensity increasing towards the centre of the coordinate space compared to gammas. This suggests a favourable region of the scintillator volume where neutrons can be counted with reduced competition from background gammas and provides a measurable metric by which to locate it for any scintillator.

The ability to measure position coordinates alongside complete pulse information unlocks the ability to quantify the anisotropy of derived properties such as particle type and energy. The ability to quantify anisotropy in measured pulse data allows study of how pulse parameters and metrics such as FoM vary across the scintillator volume. This enables events to be selected or rejected based on regional pulse properties rather than by applying an energy threshold. This has the potential to allow FoM to be optimised in-field using real event data according to specific situational requirements while still retaining the full-spectrum measuring capabilities of the detector and therefore providing more accurate measurements of neutron flux properties.

References

- [1] S. A. Pozzi et al., "Correlated neutron emissions from 252Cf", Nucl. Sci. & Eng., Vol. 178: pp. 250-260, 2014.
- [2] M. J. Joyce et al., "Real-time, digital pulse-shape discrimination in non-hazardous fast liquid scintillation detectors Prospects for safety and security", In Proc. ANIMMA, 2011.
- [3] M. J. I. Balmer, K. A. A. Gamage, G. C. Taylor, "Comparative analysis of pulse shape discrimination methods in a 6Li loaded plastic scintillator", Nucl. Inst. & Meth. A, Vol. 788: pp. 146-153, 2015.
- [4] M.J. Cieślak et al., "Pulse shape discrimination characteristics of stilbene crystal, pure and 6Li loaded plastic scintillators for a high resolution coded-aperture neutron imager", JINST 12, 2017.
- [5] C. S. Sosa et al., "Improved neutron–gamma discrimination at low-light output events using conical transstilbene," Nucl. Inst. & Meth. A, Vol. 916: pp. 42–46, 2019.
- [6] A. Parker and M. Aspinall, "Optimising Detecting Geometry for Improved Pulse Shape Discrimination Performance in Plastic Scintillation," In Proc. ANIMMA 2021.
- [7] F. Begin, G. Assaillit, and J. E. Groetz, "New shapes for liquid scintillation detectors used in neutron spectrometry," Nucl. Inst. & Meth. A, Vol. 562, no. 1, pp. 351–357, 2006.
- [8] C. S. Sosa et al., "Energy resolution experiments of conical organic scintillators and a comparison with Geant4 simulations," Nucl. Inst. & Meth. A, Vol. 898: pp. 77–84, 2018.
- [9] S. F. Naeem et al., "Spatial response characterization of liquid scintillator detectors using collimated gammaray and neutron beams", Nucl. Inst. & Meth. A, Vol. 726: pp. 120-126, 2013.
- [10] V. Popov, S. Majewski, "A compact high performance readout electronics solution for H9500 Hamamatsu 256 Multianode Photomultiplier Tube for application in gamma cameras", In Proc. IEEE NSS, pp. 2981-2985, 2006.
- [11] R. Massari, A. D'Elia, A. Soluri, "Preliminary results on a small animal SPECT system based on H13700 PSPMT coupled with CRY018 array," Nucl. Inst. & Meth. A, Vol. 940: pp 296-301, 2019.
- [12] J. -W. Son et al., "Development and Performance Evaluation of a Time-of-Flight Positron Emission Tomography Detector Based on a High-Quantum-Efficiency Multi-Anode Photomultiplier Tube", IEEE Trans. on Nucl. Sci., vol. 63, no. 1, pp. 44-51, Feb. 2016.
- [13] S. Mukhopadhyay, R. Maurer, P. Guss, "Use of a position-sensitive multi-anode photomultiplier tube for finding gamma-ray source direction", DOE/NV/25946—2150, 2014.
- [14] V. Popov, P. Degtiarenko, I. Musatov, "New detector for use in fast neutron radiography", JINST 6 C01029, 2011.

Journal of Physics: Conference Series 3130 (2025) 012006

doi:10.1088/1742-6596/3130/1/012006

- [15] C. Trotta, "High-Resolution Imaging System (HiRIS) based on H9500 PSPMT", Nucl. Inst. & Meth. A, Vol. 593: pp. 454-458, 2008.
- [16] E. Aguiló et al., "Test of multi-anode photomultiplier tubes for the LHCb scintillator pad detector", Nucl. Inst. & Meth. A, Vol. 538: pp. 255-264, 2005.
- [17] M. Machida et al., "Development of prototype RICH detector with multi-anode photomultipliers for radioactive ions", Nucl. Inst. & Meth. A, Vol. 931: pp. 23-28, 2019.
- [18] D. Freedman, P. Diaconis, "On the histogram as a density estimator: L2 theory", Probab. Theory & Relat. Fields., Vol. 57: pp. 453–476, 1981.
- [19] K. Pearson, "On the criterion that a given system of deviations from the probable in the case of a correlated system of variables is such that it can be reasonably supposed to have arisen from random sampling", Lond. Edinb. Dubl. Phil. Mag., Vol. 50(302): pp. 157–175, 1900.